

ARTICLE

Received 29 Sep 2015 | Accepted 24 Feb 2016 | Published 31 Mar 2016

DOI: 10.1038/ncomms11139

OPEN

# Revisiting the vortex-core tunnelling spectroscopy in $\text{YBa}_2\text{Cu}_3\text{O}_{7-\delta}$

Jens Bruér<sup>1</sup>, Ivan Maggio-Aprile<sup>1</sup>, Nathan Jenkins<sup>1</sup>, Zoran Ristić<sup>1</sup>, Andreas Erb<sup>2</sup>, Christophe Berthod<sup>1</sup>, Øystein Fischer<sup>1</sup> & Christoph Renner<sup>1</sup>

The observation by scanning tunnelling spectroscopy of Abrikosov vortex cores in the high-temperature superconductor  $\text{YBa}_2\text{Cu}_3\text{O}_{7-\delta}$  (Y123) has revealed a robust pair of electron-hole symmetric states at finite subgap energy. Their interpretation remains an open question because theory predicts a different signature in the vortex cores, characterized by a strong zero-bias conductance peak. Here, we present scanning tunnelling spectroscopy data on very homogeneous Y123 at 0.4 K revealing that the subgap features do not belong to vortices: they are actually observed everywhere along the surface with high spatial and energy reproducibility, even in the absence of magnetic field. Detailed analysis and modelling show that these states remain unpaired in the superconducting phase and belong to an incoherent channel, which contributes to the tunnelling signal in parallel with the superconducting density of states.

<sup>1</sup>Department of Quantum Matter Physics, University of Geneva, 24 quai Ernest-Ansermet, 1211 Geneva 4, Switzerland. <sup>2</sup>Walther-Meissner-Institut, Bayerische Akademie der Wissenschaften, Walther-Meissner-Strasse 8, D-85748 Garching, Germany. Correspondence and requests for materials should be addressed to C.R. (email: christoph.renner@unige.ch).

The interaction responsible for high-temperature superconductivity in the cuprates has remained elusive until now. Various charge orders<sup>1–5</sup> suggest that the electron matter in these compounds experiences competing interactions, while numerous spectroscopic data support the scenario of preformed pairs gaining coherence at low temperature<sup>6–10</sup>. The vortices offer a chance to disentangle the spectral features related to pairing from those that are unrelated<sup>11</sup>. In this context, the observation of discrete states in the vortex cores<sup>12–17</sup> has been a considerable challenge for theory<sup>18–25</sup>, because the calculated tunnelling spectrum in a vortex of  $d_{x^2-y^2}$  symmetry presents a broad continuous maximum centred at zero bias not observed in the experiments.

Here we present high-resolution scanning tunnelling microscopy (STM) measurements of  $\text{YBa}_2\text{Cu}_3\text{O}_{7-\delta}$  (Y123), the first high-temperature superconductor to reveal a pair of electron-hole symmetric subgap conductance peaks when tunnelling into a vortex core<sup>12</sup>. This cuprate was chosen to revisit the vortex core spectroscopy by STM because the subgap peaks are significantly stronger than analogous low-energy spectroscopic structures reported for other cuprates<sup>16,17</sup>. It furthermore shows spatially homogeneous tunnelling spectroscopy, paramount to consistently map the spatial extent of the subgap states (SGSs) in the vicinity of vortex cores. Our study shows that these discrete states are not a specific signature of the vortex cores, but are ubiquitous in zero field, even in spectra lacking superconducting coherence (SC) peaks. These results reshuffle the cards for the vortex core description in Y123 and shed new light on its low-temperature non-superconducting state.

## Results

**Persistence of SGSs in zero field and outside vortices.** We study the low-energy spectral features of Y123 in very homogeneous conductance maps measured along the (001) surface at 0.4 K. Figure 1 shows the average of 2,704 spectra recorded over a  $120 \times 120 \text{ nm}^2$  area in zero field. The persistence of sharp features in this average demonstrates the low variability of the spectral properties across the area, as well as the low noise level of the instrument. On top of a V-shaped background with a finite zero-bias (ZB) conductance, which are common on as-grown Y123 surfaces, we identify five robust particle-hole symmetric

spectroscopic features as labelled in Fig. 1. We shall not discuss here the hump, the dip and the pseudogap (PG), but focus on the SC peaks near  $\pm 17 \text{ meV}$ , and especially on the SGSs at  $\pm 5 \text{ meV}$ . We confirm the surface homogeneity by studying the spatial and statistical distributions of the superconducting gap  $\Delta_{\text{SC}}$ , defined as half the energy separation between the two SC peaks (Fig. 1b,c). The average gap is  $17.2 \text{ meV}$  with a standard deviation of  $1.9 \text{ meV}$ , corresponding to a ratio  $2\Delta_{\text{SC}}/k_{\text{B}}T_{\text{c}} = 4.34 \pm 0.5$ , where  $k_{\text{B}}$  is the Boltzmann constant and  $T_{\text{c}}$  is the critical temperature. This gap uniformity in Y123 contrasts with the case of Bi-based cuprates, where up to 50% inhomogeneity is often observed in the gap values, even at optimal doping and for samples with sharp superconducting transitions. Most remarkable in Fig. 1 are the SGSs at  $\pm 5 \text{ meV}$ . Until now, this structure had only been clearly resolved as peaks inside the vortices<sup>12,15</sup>. Much weaker subgap shoulders were occasionally observed in zero field or outside vortices. The natural interpretation has been that the structure would be strongly enhanced in the vortex cores, suggestive of a phenomenon competing with superconductivity. Our measurements show that this is not the case: the structure is as strong in zero field as it is in the vortex cores. The well-defined subgap peaks in the average spectrum show that the energy of this structure does not vary appreciably along the surface.

Applying a field of 6 T perpendicular to the Cu-O planes, we observe vortices as shown in Fig. 2a. The vortices are imaged by mapping the ratio of the conductance at 5 and 17 meV, denoted as  $\sigma_{\text{SGS}}/\sigma_{\text{SC}}$ . Outside the vortices, the coherence peaks are well developed and the ratio is typically 0.75; this is slightly larger than the value in zero field (0.7), because the SC peaks are smeared due to nearby vortices. Inside the vortices, the ratio increases up to values above unity as the coherence peaks get totally suppressed. The spatial evolution of the conductance from the vortex core to the inter-vortex region (Fig. 2b) shows unambiguously that the SGS feature is not localized inside vortices, and is the same structure as the one seen in zero field. The outstanding features of this trace are independent of direction away from the vortex core, although their relative amplitudes do depend on the proximity of neighbouring cores.

**Absence of correlation between SGSs and vortices.** Figure 2b gives the visual impression that the SGS peaks are reinforced in the vortex. Upon closer inspection, this turns out to be an illusion created by the suppression of the coherence peaks in the core. In fact, the PG, dip, hump and background all remain virtually unchanged upon entering the vortex. The only noticeable spectral changes along the way are an increase of the ZB conductance and a suppression of the coherence peaks. The ZB conductance has a spatial distribution analogous to the conductance ratio  $\sigma_{\text{SGS}}/\sigma_{\text{SC}}$  displayed in Fig. 2a, although with a weaker contrast. This is illustrated in Fig. 3a, which shows a good statistical correlation between the ZB conductance and  $\sigma_{\text{SGS}}/\sigma_{\text{SC}}$ , both increasing when approaching the vortex core at  $d = 0$ . As expected for a weakening superconducting order parameter inside vortices, we find a clear negative correlation between the SC peak height and  $\sigma_{\text{SGS}}/\sigma_{\text{SC}}$ . To quantify the amount of correlation between the SGS and the vortex position, we define the amplitude of the SGS as their height above the ZB conductance, measured by the difference  $\sigma_{\text{SGS}} - \sigma_{\text{ZB}}$ . As illustrated in Fig. 3c, the amplitude of the SGSs is completely uncorrelated with the vortices. This is our central result.

## Discussion

The good correlation between the SC peaks and  $\sigma_{\text{SGS}}/\sigma_{\text{SC}}$  and the absence of correlation between the SGS and  $\sigma_{\text{SGS}}/\sigma_{\text{SC}}$  imply that there is no correlation between the SGS and the SC peak, as we

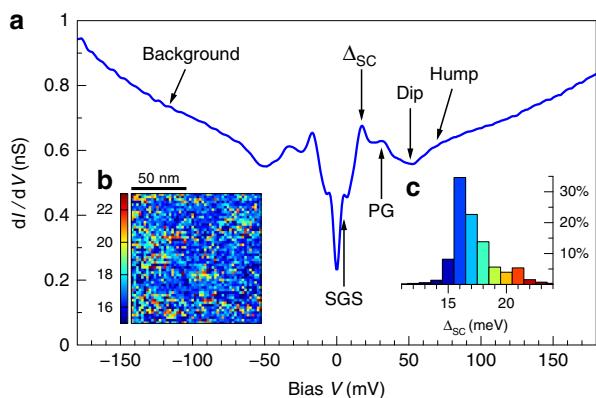


**Figure 1 | Subgap states are observed in zero field.** (a) Average  $dI/dV$  conductance of a  $120 \times 120 \text{ nm}^2$  area at  $T = 0.4 \text{ K}$  in zero field. The junction resistance was  $1.2 \text{ G}\Omega$  and the regulation voltage  $300 \text{ mV}$ . Five electron-hole symmetric spectral features and the background are indicated. (b) Spatial map of the superconducting gap  $\Delta_{\text{SC}}$  over the same area. (c) Histogram of the gap values shown in b. The colouring of bars corresponds to the colour scale shown in b.

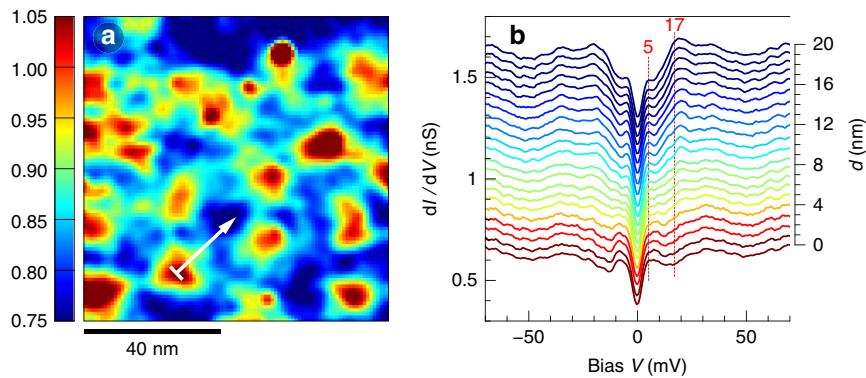


**Figure 2 | The subgap states exist inside and outside vortices.** (a) Ratio  $\sigma_{\text{SGS}}/\sigma_{\text{SC}}$  of the conductances at 5 and 17 meV measured at  $T=0.4\text{ K}$  in a 6 T field over a  $90 \times 90\text{ nm}^2$  area. The vortex cores appear in red and the inter-vortex regions in blue. The white arrow indicates a 20-nm path starting in a vortex core. (b) Conductance spectra along the white arrow shown in a. The spectra are coloured according to the conductance ratio  $\sigma_{\text{SGS}}/\sigma_{\text{SC}}$ . The conductance scale is shown for the bottom spectrum; the others are displaced vertically by 0.05 nS for visibility. The distance  $d$  to the core is shown on the right axis. The red dashed lines mark the energies 5 and 17 meV.

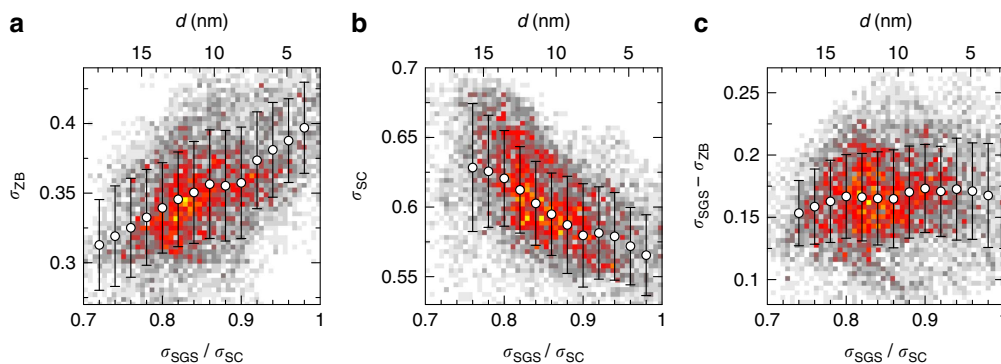


**Figure 3 | Correlation of spectral features and distance from vortex-core centre.** The conductance ratio  $\sigma_{\text{SGS}}/\sigma_{\text{SC}}$  evaluated along the white arrow of Fig. 2a provides a measure of the distance  $d$  from the vortex centre. We find a strong correlation between this distance and (a) the zero-bias conductance and (b) the conductance at  $\Delta_{\text{SC}}$ , but not with (c) the amplitude of the subgap states. The colour plots are histograms showing the frequency of each pair of values on the same area as in Fig. 2a (white-grey: low; red-yellow: high). The circles and error bars indicate the average and the standard deviation of the distributions at fixed values of the conductance ratio.

have verified in the experimental data. Figure 4 confirms the lack of sensitivity of the SGS to the SC. A vortex-core spectrum (Fig. 4a) is compared with two zero-field spectra without coherence peaks, at a twin boundary<sup>26</sup> (Fig. 4b), and inside an extended region of the sample surface where no SC was detected (Fig. 4c). All three spectra present the SGS feature at the same energy on top of different backgrounds. The PG feature appears to be also present in all three cases.

STM topography reveals atomically flat terraces (roughness below 0.2 nm) separated by full (1.2 nm) or fractional (0.4–0.8 nm) unit-cell steps as well as twin boundaries. The absence of atomic resolution prevents a positive identification of the surface layer. But it does not preclude the interpretation of the tunnelling spectra in terms of intrinsic superconducting Y123 properties as the following compelling evidences show. The gap defined by the coherence peaks satisfies the characteristic features expected for the superconducting gap of bulk Y123: its amplitude matches other bulk probes and  $2\Delta_{\text{SC}}/k_{\text{B}}T_{\text{c}}$  is in close agreement with the weak-coupling Bardeen-Cooper-Schrieffer (BCS) value of 4.3 for an order parameter of  $d_{x^2-y^2}$  symmetry; the coherence peaks vanish upon warming through the bulk superconducting transition temperature, in the vicinity of twin boundaries, and when entering a vortex core. The very high reproducibility of the

other spectral features as a function of surface preparation, time, applied magnetic field, distance from vortex cores, step edges and twin boundaries makes it extremely unlikely that they reflect electronic surface states. The latter are usually not as robust and one would expect modifications near step edges and twin boundaries. Last, there is a perfect match between the superconducting gap features measured by STM and point contact Andreev–Saint-James spectroscopy, as expected<sup>27</sup>. This body of evidences unquestionably links  $\Delta_{\text{SC}}$  with Y123 bulk superconductivity and rules out electronic surface states to explain the other features. We can also exclude that the SGS mark a proximity-induced or mixed  $d+s$  or  $d+is$  order parameter. In that case, the SGS would shift to lower energy and ultimately disappear when approaching the vortex centres where phase coherence is lost, in clear contradiction with our data. Finally, the persistence of the SGS excludes their interpretation as vortex-core states or features of another state that would compete with superconductivity and pop up in the vortices.

An obvious question is whether the non-superconducting spectra shown in Fig. 4 represent the normal-state density of states (DOS) from which superconductivity emerges. Considering an isotropic normal state (that is, with dispersion  $E_{\mathbf{k}}$  depending only on the modulus of  $\mathbf{k}$ ) characterized by a DOS  $N_0(E)$ , we find

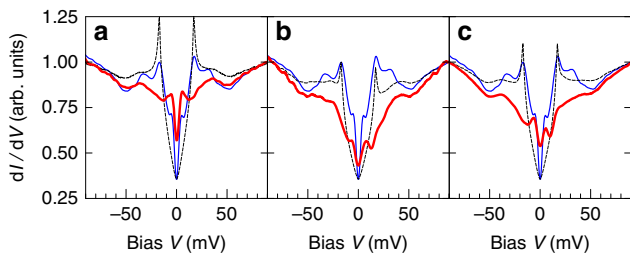


**Figure 4 | The subgap states survive the loss of coherence.** The thick red curves show the tunnelling conductance measured at  $T = 0.4$  K in (a) a vortex core (6 T field), (b) at a twin boundary (zero field) and (c) in a non-superconducting region (zero field). The thin blue lines show a typical averaged zero-field spectrum. The dashed lines show that the model (1) with the red curve as  $N_0(\xi)$  is inconsistent with the zero-field data; a constant was added to match the zero-bias conductance at zero-field. All curves are normalized to unity at the right edge of the graph.

that, in the presence of a  $d$ -wave order parameter  $\Delta \cos(2\theta)$ , the BCS DOS can be written as

$$N(E) = \int_{-\infty}^{\infty} d\xi N_0(\xi) \left( -\frac{1}{\pi} \right) \times \text{Im} \left[ \frac{E + i\Gamma + \xi}{\sqrt{(E + i\Gamma)^2 - \xi^2} \sqrt{(E + i\Gamma)^2 - \xi^2 - \Delta^2}} \right]. \quad (1)$$

The derivation is given in Supplementary Note 1. Taking the spectra of Fig. 4 for  $N_0(\xi)$ ,  $\Delta = 17$  meV and  $\Gamma = 0.5$  meV, we obtain the superconducting DOS shown as dashed lines in each panel. It is clear that the SGS are completely washed out, unlike in the experiment (Fig. 1). A feature of the normal-state DOS at energy  $\xi$  indeed gets spread over an energy range  $[\xi, \sqrt{\xi^2 + \Delta^2}]$  by the  $d$ -wave gap: high-energy features like the PG at  $\xi \gg \Delta$  remain sharp, but low-energy features are typically smeared over a range  $\Delta$ . Illustrations can be found in Supplementary Fig. 1.

The picture emerging from our data is that the SGS exist independently of magnetic field and are not affected by the opening of the superconducting gap. Two possible scenarios are compatible with the latter observation: the SGS either belong to an atomic layer different from the superconducting copper oxide planes or they are confined to the nodal regions in momentum space in the superconducting layers. In the first scenario, the tunnelling spectrum would be a superposition of two distinct contributions: one from non-superconducting electrons characterized by the robust and homogeneous SGS as well as the ubiquitous high ZB conductance, another from the superconducting condensate responsible for the fragile coherence peaks. Indeed, the spectrum of Fig. 1 can be perfectly reproduced by summing a pure  $d$ -wave spectrum and a background conductance similar to the spectra of Fig. 4 (see the Methods for details). In this model, the background forms the dominant spectral contribution to account for the large ZB and V-shaped background conductances systematically observed in Y123 tunnelling spectra. It may also explain why the vortex cores do not show the expected BCS spectrum (Fig. 2b). Note that our data does show an increase of the ZB conductance in the cores (Figs 3a and 4a), which may well be related to the predicted  $d$ -wave ZB anomaly that is obscured by the SGS.

The second scenario assumes the SGS coexist with the superfluid condensate in the copper oxide planes. Then, the SGS have to be confined to the nodal regions in momentum space where the superconducting gap is small. Otherwise, they would have to shift or broaden like in Fig. 4 as the gap opens in the superconducting regions, in contradiction with the observations in Figs 1 and 2. Supplementary Fig. 2 presents a toy model

exhibiting this property. A recent study reports particular spectroscopic signatures from the nodal regions in momentum space, however, without an obvious link to the SGS<sup>28</sup>.

In either scenario it is tempting to link the SGS with the static charge density wave discovered recently in Y123 (refs 3,4). On one hand, the temperature scale of this phenomenon ( $\sim 100$  K at optimal doping, see for example, ref. 29) agrees well with the energy separation between the SGS peaks. On the other hand, seemingly similar subgap structures observed in Bi2212 vortices<sup>14</sup> display a modulated real-space pattern<sup>1,16,17</sup>. An explicit link between such conductance patterns seen by STM and the charge density wave was demonstrated in Bi2201 (ref. 5). Preliminary data suggest similar real-space modulation of the SGS in Y123, but further experiments are under way.

In summary, we report the observation by STM of low-energy ( $\pm 5$  meV) particle-hole symmetric states in Y123. These states, seen previously only in vortex cores, are in fact a robust property of Y123, insensitive to the magnetic field and to the SC. The SGSs often take the form of peaks in the tunnelling spectrum when the SC peaks are absent, but thanks to high-resolution measurements we also see them as peaks even in spectra with SC peaks. This new phenomenology redefines the question of the spectroscopy of vortices in the cuprates. Whether the new energy scale is a pairing scale, as its particle-hole symmetry suggests, whether it is connected to the Cu-O chains or has to do with some charge ordering, as suggested by similar features in Bi2212, remain open questions at this stage.

## Methods

**Sample preparation.** The experiments were conducted on as-grown (001) surfaces of highly pure  $\text{YBa}_2\text{Cu}_3\text{O}_{7-\delta}$  single crystals, grown in  $\text{BaZrO}_3$  crucibles<sup>30</sup>. The samples were annealed in pure oxygen to reach an optimal doping with  $T_c = 92$  K. Both as-grown and chemically etched surfaces were investigated. As-grown surfaces were simply rinsed in ethanol in an ultrasonic bath before insertion into the STM. Chemical etching was done by immersion for 1 min in a solution of 1% bromine and 99% ethanol, followed by rinsing in ethanol and transfer to the vacuum chamber with less than 5 min exposure to air. All data reported here were measured on as-grown surfaces, except the spectra in Fig. 4b,c, which were measured on chemically etched surfaces. The spectra are independent of surface preparation. They are reproducible over time and after repeated thermal cycling and exposure to air on untreated surfaces, and likewise on etched surfaces if the etching is repeated.

**High-resolution STS measurements.** We used a home-built high-vacuum variable temperature STM optimized for high energy resolution, with a base temperature of 0.4 K, and chemically etched tips made of pure iridium. Tunnelling spectra were acquired in zero magnetic field and in a field of 6 T oriented along the surface normal. The  $dI/dV$  curves, providing a measure of the electronic local density of states, were obtained by numerical differentiation of the measured  $I(V)$  characteristics. For measurements done on as-grown surfaces, the junction resistance was increased to 12 G $\Omega$  when moving the tip over these surfaces (as opposed to 1.2 G $\Omega$  in the spectroscopy mode), in order to avoid that contaminants stick to the tip during its motion. For the etched surfaces, the junction resistance was kept at 1.2 G $\Omega$  during scanning and spectroscopy. Both procedures result in atomically flat surfaces allowing reproducible imaging and spectroscopy.

**Two-channel model for the Y123 spectrum.** We assume that the Y123 tunnelling spectrum gets parallel contributions from a two-dimensional band distorted by the coupling to spin excitations and subject to conventional BCS  $d$ -wave pairing, and from a non-superconducting incoherent bath:

$$\frac{dI}{dV} = M_d N_d(eV) + M_b N_b(eV). \quad (2)$$

$N_d(E)$  is the DOS of the BCS band and  $M_d$  represents the tunnelling matrix element for this band, whereas  $M_b$  and  $N_b(E)$  are the matrix element and the DOS for the non-superconducting bath, respectively. In the non-superconducting regions of the surface, the coherent band turns normal with a DOS  $N_0(E)$  and the differential conductance becomes

$$\left( \frac{dI}{dV} \right)_{\text{ns}} = M'_d N_0(eV) + M'_b N_b(eV) \approx \left( \frac{dI}{dV} \right)_{\text{core}}. \quad (3)$$

The matrix elements are in general different in the two types of regions: the constant-current STM setpoint regulation may change the relative contributions of



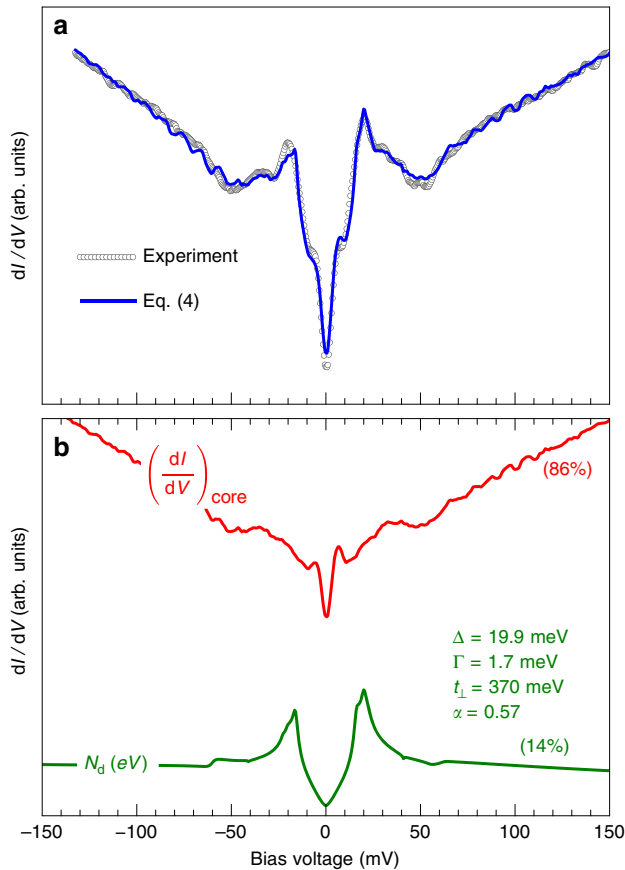


**Figure 5 | Two-channel model for  $\text{YBa}_2\text{Cu}_3\text{O}_{7-\delta}$ .** (a) Best fit (solid blue line) of the model (4) to the tunnelling spectrum of Y123 measured between vortices. (b) Comparison of the coherent (green) and incoherent (red) contributions to the total spectrum. The numbers in parentheses give their relative contributions to the total spectral weight in the energy range of the figure.

the two channels when the coherent band becomes normal and its mobility drops. We will assume that the spectrum measured in the vortex cores is a good approximation for the spectrum of non-superconducting regions. Eliminating  $N_b(E)$  from equation (2) by means of equation (3), we are left with the model

$$\frac{dI}{dV} = \frac{M_b}{M_b} \left[ \left( \frac{dI}{dV} \right)_{\text{core}} - M'_d N_0(E) \right] + M_d N_d(E). \quad (4)$$

We calculate  $N_d(E)$  and  $N_0(E)$  for a two-dimensional square lattice with a dispersion that reproduces the basic fermiology of Y123. For the tight-binding parameters of the bonding band reported in ref. 31. For simplicity, we ignore the fourth and fifth neighbour hopping amplitudes and adjust the chemical potential in order to reach a hole concentration of 0.16. The resulting parameters are  $(t_1, t_2, t_3, \mu) = (-281, 139, -44, -356)$  meV. Y123 is a bi-layer material with both bonding and anti-bonding bands, but there is considerable uncertainty regarding the precise properties of the anti-bonding band. We add an anti-bonding band via a bilayer coupling  $t_{\perp}$  and determine  $t_{\perp}$  by least-square fitting. The two-band model for the dispersion is

$$E_{\mathbf{k}}^{\pm} = 2t_1 (\cos k_x + \cos k_y) + 4t_2 \cos k_x \cos k_y + 2t_3 (\cos 2k_x + \cos 2k_y) \pm \frac{t_{\perp}}{4} (\cos k_x - \cos k_y)^2 - \mu. \quad (5)$$

The interaction with the spin resonance is included using the approach described in ref. 32. Beside its energy  $\Omega_s = 41$  meV, the parameters that characterize the spin resonance are its energy width  $\Gamma_s$  and momentum width  $\Delta q$ . As the resonance is sharp in Y123, we set  $\Gamma_s = 0$ . The resonance has a full-width at half-maximum  $0.26 \text{ \AA}^{-1} \approx 1/a$ , with  $a$  the in-plane lattice parameter of Y123. We therefore take  $\Delta q = 1/a$ . The only remaining free parameter is a dimensionless coupling  $\alpha$  between the Bogoliubov-de Gennes quasiparticles and the spin mode<sup>33</sup>. We determine the matrix elements  $M_b/M'_b, M'_d, M_d$ , the model parameters  $t_{\perp}$  and  $\alpha$ , as well as the gap  $\Delta$  and Dynes broadening  $\Gamma$  by least-square fitting of the equation (4) to the DOS measured in-between vortices, which is very similar to the zero-field spectrum shown in Fig. 1.

The result of the fit is displayed in Fig. 5, where the fitted parameters are also reported. The fit yields  $M'_d = 0$ , indicating that the coherent band is indeed invisible when it becomes normal; this supports an interpretation that this band would lie in the CuO plane below the surface and show up in the STM conductance only when it superconducts. The model captures well the asymmetric heights of the coherence peaks, the relative value of the ZB and background conductances, and the dips at positive and negative energies. Further refinements of the model, for instance by allowing the adjustment of all band parameters, could presumably improve the agreement even further.

## References

- Hoffman, J. E. *et al.* A four unit cell periodic pattern of quasi-particle states surrounding vortex cores in  $\text{Bi}_2\text{Sr}_2\text{CaCu}_2\text{O}_{8+\delta}$ . *Science* **295**, 466–469 (2002).
- Lawler, M. J. *et al.* Intra-unit-cell electronic nematicity of the high- $T_c$  copper-oxide pseudogap states. *Nature* **466**, 347–351 (2010).
- Ghiringhelli, G. *et al.* Long-range incommensurate charge fluctuations in  $(\text{Y,Nd})\text{Ba}_2\text{Cu}_3\text{O}_{6+x}$ . *Science* **337**, 821–825 (2012).
- Chang, J. *et al.* Direct observation of competition between superconductivity and charge density wave order in  $\text{YBa}_2\text{Cu}_3\text{O}_{6.67}$ . *Nat. Phys.* **8**, 871–876 (2012).
- Comin, R. *et al.* Charge order driven by Fermi-arc instability in  $\text{Bi}_2\text{Sr}_2-x\text{La}_x\text{CuO}_{6+\delta}$ . *Science* **343**, 390–392 (2014).
- Renner, C., Revaz, B., Genoud, J.-Y., Kadowaki, K. & Fischer, Ø. Pseudogap precursor of the superconducting gap in under- and overdoped  $\text{Bi}_2\text{Sr}_2\text{CaCu}_2\text{O}_{8+\delta}$ . *Phys. Rev. Lett.* **80**, 149–152 (1998).
- Kanigel, A. *et al.* Evidence for pairing above the transition temperature of cuprate superconductors from the electronic dispersion in the pseudogap phase. *Phys. Rev. Lett.* **101**, 137002 (2008).
- Yang, H.-B. *et al.* Emergence of preformed Cooper pairs from the doped Mott insulating state in  $\text{Bi}_2\text{Sr}_2\text{CaCu}_2\text{O}_{8+\delta}$ . *Nature* **456**, 77–80 (2008).
- Mishra, V., Chatterjee, U., Campuzano, J. C. & Norman, M. R. Effect of the pseudogap on the transition temperature in the cuprates and implications for its origin. *Nat. Phys.* **10**, 357–360 (2014).
- Kondo, T. *et al.* Point nodes persisting far beyond  $T_c$  in  $\text{Bi}2212$ . *Nat. Commun.* **6**, 7699 (2015).
- Fischer, Ø., Kugler, M., Maggio-Aprile, I., Berthod, C. & Renner, C. Scanning tunneling spectroscopy of high-temperature superconductors. *Rev. Mod. Phys.* **79**, 353–419 (2007).
- Maggio-Aprile, I., Renner, C., Erb, A., Walker, E. & Fischer, Ø. Direct vortex lattice imaging and tunneling spectroscopy of flux lines on  $\text{YBa}_2\text{Cu}_3\text{O}_{7-\delta}$ . *Phys. Rev. Lett.* **75**, 2754–2757 (1995).
- Renner, C., Revaz, B., Kadowaki, K., Maggio-Aprile, I. & Fischer, Ø. Observation of the low temperature pseudogap in the vortex cores of  $\text{Bi}_2\text{Sr}_2\text{CaCu}_2\text{O}_{8+\delta}$ . *Phys. Rev. Lett.* **80**, 3606–3609 (1998).
- Hoogenboom, B. W., Renner, C., Revaz, B., Maggio-Aprile, I. & Fischer, Ø. Low-energy structures in vortex core tunneling spectra in  $\text{Bi}_2\text{Sr}_2\text{CaCu}_2\text{O}_{8+\delta}$ . *Physica C* **332**, 440–444 (2000).
- Shibata, K., Nishizaki, T., Maki, M. & Kobayashi, N. Local spectroscopy and vortex-core imaging on chemically wet-etched surfaces of  $\text{YBa}_2\text{Cu}_3\text{O}_y$  by scanning tunneling microscopy/spectroscopy. *Supercond. Sci. Technol.* **23**, 085004 (2010).
- Levy, G., Kugler, M., Manuel, A. A., Fischer, Ø. & Li, M. Fourfold structure of vortex-core states in  $\text{Bi}_2\text{Sr}_2\text{CaCu}_2\text{O}_{8+\delta}$ . *Phys. Rev. Lett.* **95**, 257005 (2005).
- Yoshizawa, S. *et al.* High-resolution scanning tunneling spectroscopy of vortex cores in inhomogeneous electronic states of  $\text{Bi}_2\text{Sr}_2\text{CaCu}_2\text{O}_x$ . *J. Phys. Soc. Jpn* **82**, 083706 (2013).
- Arovas, D. P., Berlinsky, A. J., Kallin, C. & Zhang, S.-C. Superconducting vortex with antiferromagnetic core. *Phys. Rev. Lett.* **79**, 2871–2874 (1997).
- Franz, M. & Tešanović, Z. Self-consistent electronic structure of a  $d_{x^2-y^2}$  and a  $d_{xy}$  vortex. *Phys. Rev. Lett.* **80**, 4763–4766 (1998).
- Andersen, B. M., Bruus, H. & Hedegård, P. SO(5) theory of insulating vortex cores in high- $T_c$  materials. *Phys. Rev. B* **61**, 6298–6302 (2000).
- Kishine, J.-i., Lee, P. A. & Wen, X.-G. Staggered local density-of-states around the vortex in underdoped cuprates. *Phys. Rev. Lett.* **86**, 5365–5368 (2001).
- Berthod, C. & Giovannini, B. Density of states in high- $T_c$  superconductor vortices. *Phys. Rev. Lett.* **87**, 277002 (2001).
- Zhu, J.-X. & Ting, C. S. Quasiparticle states at a  $d$ -wave vortex core in high- $T_c$  superconductors: Induction of local spin density wave order. *Phys. Rev. Lett.* **87**, 147002 (2001).
- Tsuchiura, H., Ogata, M., Tanaka, Y. & Kashiwaya, S. Electronic states around a vortex core in high- $T_c$  superconductors based on the  $t$ - $J$  model. *Phys. Rev. B* **68**, 012509 (2003).
- Fogelström, M. Structure of the core of magnetic vortices in  $d$ -wave superconductors with a subdominant triplet pairing mechanism. *Phys. Rev. B* **84**, 064530 (2011).
- Deutscher, G. & Müller, K. A. Origin of superconductive glassy state and extrinsic critical currents in high- $T_c$  oxides. *Phys. Rev. Lett.* **59**, 1745–1747 (1987).

27. Deutscher, G. Coherence and single-particle excitations in the high-temperature superconductors. *Nature* **397**, 410–412 (1999).
28. Sebastian, S. E. *et al.* Normal-state nodal electronic structure in underdoped high- $T_c$  copper oxides. *Nature* **511**, 61–64 (2014).
29. Blanco-Canosa, S. *et al.* Resonant X-ray scattering study of charge-density wave correlations in  $\text{YBa}_2\text{Cu}_3\text{O}_{6+x}$ . *Phys. Rev. B* **90**, 054513 (2014).
30. Erb, A., Walker, E. & Flükiger, R.  $\text{BaZrO}_3$ : the solution for the crucible corrosion problem during the single crystal growth of high- $T_c$  superconductors  $\text{REBa}_2\text{Cu}_3\text{O}_{7-\delta}$ ; RE = Y, Pr. *Physica C Supercond.* **245**, 245–251 (1995).
31. Schabel, M. C. *et al.* Angle-resolved photoemission on untwinned  $\text{YBa}_2\text{Cu}_3\text{O}_{6.95}$ . I. electronic structure and dispersion relations of surface and bulk bands. *Phys. Rev. B* **57**, 6090–6106 (1998).
32. Eschrig, M. The effect of collective spin-1 excitations on electronic spectra in high- $T_c$  superconductors. *Adv. Phys.* **55**, 47–183 (2006).
33. Berthod, C. *et al.* Strong-coupling analysis of scanning tunneling spectra in  $\text{Bi}_2\text{Sr}_2\text{Ca}_2\text{Cu}_3\text{O}_{10+\delta}$ . *Phys. Rev. B* **88**, 014528 (2013).

## Acknowledgements

We acknowledge discussions with G. Deutscher and S.-H. Pan. We thank A. Guipet and L. Stark for their technical assistance. This research was supported by the NCCR MaNEP and the Swiss National Science Foundation.

## Author contributions

Ø.F., I.M.-A. and C.R. designed the experiments. A.E. grew the samples. J.B., N.J., Z.R. and I.M.-A. carried out the measurements. J.B., C.B., N.J., I.M.-A. and C.R. performed the data analysis and wrote the manuscript. C.B. did the theoretical modelling.

## Additional information

**Supplementary Information** accompanies this paper at <http://www.nature.com/naturecommunications>

**Competing financial interests:** The authors declare no competing financial interests.

**Reprints and permission** information is available online at <http://npg.nature.com/reprintsandpermissions/>

**How to cite this article:** Bruér, J. *et al.* Revisiting the vortex-core tunnelling spectroscopy in  $\text{YBa}_2\text{Cu}_3\text{O}_{7-\delta}$ . *Nat. Commun.* **7**:11139 doi: 10.1038/ncomms11139 (2016).



This work is licensed under a Creative Commons Attribution 4.0 International License. The images or other third party material in this article are included in the article's Creative Commons license, unless indicated otherwise in the credit line; if the material is not included under the Creative Commons license, users will need to obtain permission from the license holder to reproduce the material. To view a copy of this license, visit <http://creativecommons.org/licenses/by/4.0/>